Article:
Knight, JW, Egan, JV, Orr-Ewing, AJ et al. (2022) Direct Spectroscopic Quantification of the Absorption and Scattering Properties for Single Aerosol Particles. The Journal of Physical Chemistry A, 126 (9). pp. 1571-1577. ISSN: 1089-5639

https://doi.org/10.1021/acs.jpca.2c00532

Direct Spectroscopic Quantification of the Absorption and Scattering Properties for Single Aerosol Particles

Jamie W. Knight,[1] Joanna V. Egan,[1,2] Andrew J. Orr-Ewing,[1]* Michael I. Cotterell[1]*

[1]School of Chemistry, University of Bristol, Cantock's Close, Bristol, UK, BS8 1TS
[2]School of Chemistry, University of Leeds, Woodhouse Lane, Leeds, UK, LS2 9JT

**Correspondence to*:
Michael I. Cotterell (m.cotterell@bristol.ac.uk)
Andrew J. Orr-Ewing (a.orr-ewing@bristol.ac.uk)

Abstract

Understanding the optical properties of micrometre-scale light absorbing aerosol particles is of paramount importance to address key challenges in atmospheric and physical chemistry. For example, absorption of solar radiation by atmospheric aerosols represents one of the largest uncertainties in climate models. Moreover, reaction acceleration within the unique environments of aerosol droplets cannot be replicated in bulk solutions. The causes of these reaction rate enhancements remain controversial, but ultra-sensitive spectroscopic measurements of evolving aerosol optical properties should provide new insights. We demonstrate a new approach using cavity ring-down spectroscopy that allows the first direct spectroscopic quantification of the continuously evolving absorption and scattering cross sections for single, levitated, micrometre-scale particles as their size and chromophore concentration change. For two-component droplets composed of nigrosin and 1,2,6-hexanetriol, the unprecedented sensitivity of our measurements reveals the evolving real and imaginary components of the refractive index caused by changes in concentration as 1,2,6-hexanetriol slowly evaporates.

Introduction

Atmospheric aerosols affect climate through their interactions with solar and terrestrial radiation. However, large uncertainties persist in the magnitudes of the scattering and absorption of incident radiation by these atmospheric particles, particularly for aerosols such as brown carbon (BrC) particulates comprised of organic species that absorb solar radiation at visible wavelengths.[1] The complex refractive index, $m = n + ik$, quantifies the intensive optical properties of the material constituting an aerosol particle, with the real component n dependent on the mean molecular polarizability and density of the particle, and the imaginary component k characterizing the attenuation (absorption) of light. Accurate and sensitive measurements of the complex refractive indices for absorbing aerosol species are urgently needed to improve current descriptions of the impact of aerosols in atmospheric and climate models.[1-3] Such measurements should also be able to explore the complex atmospheric aging of aerosols, which will be influenced by multiphase chemical processes, photoinitiated chemical reactions within the particles, and gas-particle partitioning of semi-volatile species. Moreover, spectroscopic monitoring of m could provide critical insights into how the unique physicochemical properties of aerosol particles affect reaction rates,[4] including attributions of accelerated rates to specific properties of the particle and its ambient environment.[5, 6]

Single aerosol particle spectroscopy offers greater accuracy and precision in determination of complex refractive indices than measurements on ensembles of particles.[7-9] Combining this single-particle spectroscopy with particle trapping and levitation then enables the study of processes occurring on timescales relevant to atmospheric aerosols, which can have lifetimes of several days. Such extended measurements are beyond typical atmospheric chamber approaches. Photoacoustic spectroscopy (PAS) has recently been combined with optical trapping techniques to measure light absorption properties for single aerosol particles,[10] but can suffer from artefacts arising from latent heat energy transfer pathways that confound data interpretation when particles contain volatile species.[11, 12] Price *et al*. instead used a linear electrodynamic quadrupole trap to confine single droplets and then recorded spectra of the elastically scattered light from an incident broadband light emitting diode light source.[13] Their approach potentially provides complex refractive indices for light absorbing aerosol droplets across a range of wavelengths, although the accuracy and precision of these retrievals is not yet clear for light absorbing droplets.[14] Similarly, Bluvshtein *et al.* used photophoretic spectroscopy to probe single particles with weak absorption strengths levitated in a double-ring electrodynamic balance, but the extension of these measurements to particles with absorption strengths and particle sizes relevant to many aerosol science applications is uncertain.[15] The approach we adopt uses cavity ring-down spectroscopy (CRDS) to measure the aerosol extinction cross section (σ_{ext}), the total power scattered and absorbed from an incident light beam, directly and

with high sensitivity owing to the several-kilometre path length of the probe beam inside an optical cavity.[16] Our CRDS measurements have previously provided σ_{ext} values for single *non-absorbing* aerosol particles levitated in optical traps,[17-19] but extending our studies to light-absorbing aerosols, as reported here, is a significant advance. Established optical trapping techniques are unable to confine absorbing particles spatially with the stability required for CRDS measurements because photophoretic forces displace particles away from regions of high light intensity.[20] Instead, we have recently introduced a linear electrodynamic quadrupole (LEQ) trap for the stable levitation of scattering aerosols within a CRDS spectrometer,[14] as depicted in Figure 1. The LEQ provides controlled particle levitation irrespective of absorption strength and, in combination with CRDS, enables us to characterize the optical properties of single, light absorbing particles as small as ~1 μm in diameter.

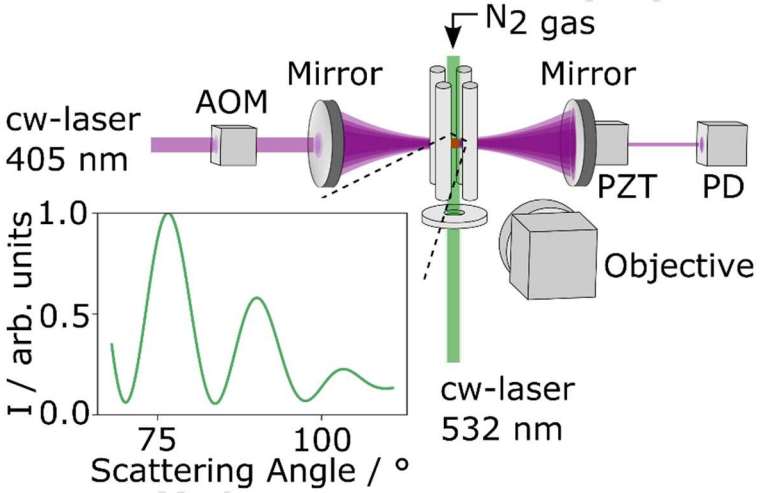

Figure 1. Schematic diagram of the single particle CRDS approach for spectroscopic interrogation at a wavelength of 405 nm of single aerosol particles levitated in an LEQ trap, with angularly resolved elastic light scattering from the 532-nm laser to retrieve particle size. AOM is an acousto-optic modulator, PZT is a piezo-electric actuator, PD is a photodiode, and I is the elastic light scattering intensity.

Herein, we demonstrate the use of an LEQ trap to levitate single absorbing particles and manipulate them into the centre of a CRDS probe laser beam. Extinction cross sections, complex refractive indices, and evolving droplet diameters are precisely determined from concurrent CRDS and elastic light scattering measurements for confined single particles with a range of absorption strengths. The retrieved *n* and *k* values agree well with predictions from physically based mixing rule models.

Experimental Methods

The experimental set-up (Figure 1) is based on our single particle cw-CRDS apparatus reported previously, but with an upgrade to the cw laser system for enhanced experimental performance.[14, 21] The beam from a 405 nm laser (Toptica Photonics, TopMode 50 mW) is passed through an acousto-optic modulator, with the first order diffraction beam coupled into a resonant mode of a high finesse optical cavity formed by two high reflectivity mirrors. One of these mirrors is mounted on a piezo-electric actuator which modulates the mirror position to tune the cavity into resonance with the narrow bandwidth (<5 MHz) laser light. On resonance, the intracavity light intensity increases and is monitored by a photodiode that detects the light transmitted through the cavity. Once a threshold photodiode voltage is reached, an electrical pulse is sent to the acousto-optic modulator to extinguish the first order diffraction beam and initiate a ring-down event. The intensity of the intracavity beam subsequently decreases exponentially. The characteristic time taken for the light intensity to decrease by a factor of $1/e$ is known as the ring-down time, τ.

In the experimental measurements reported here, aqueous solutions containing 1,2,6-hexanetriol (HT; Sigma-Aldrich; 96%) or mixtures of HT with water soluble nigrosin dye (Sigma-Aldrich, CAS code: 8005-03-6, batch number: BCBG2998V) were loaded into a droplet-on-demand dispenser placed close to an induction electrode. The induction electrode imparted an ion imbalance as ~20 μm diameter droplets were dispensed and injected into the LEQ trapping cell. N_2 gas flowing downwards through the LEQ trapping cell maintained a low relative humidity (<10%) and the water in the trapped droplets evaporated rapidly (within ~1 s) to equilibrate with this low-RH environment, leaving a droplet with a radius of ~1600 nm. An additional flow of dry HEPA-filtered N_2 passed over the faces of the cavity mirrors and along the length of the optical cavity towards the CRDS entrance apertures of the LEQ trapping cell, thereby purging the cavity of dust or light absorbing gas species that could confound our extinction measurements on single particles. The cavity was otherwise sealed from the ambient laboratory environment. Although a capability that was not exploited in the current work, this design allows the properties of the droplet's surroundings such as relative humidity to be controlled. AC voltages were applied to pairs of diametrically opposite rods of the LEQ trap, confining the particles in the horizontal plane. A voltage applied to a bottom DC electrode exerted a repulsive electrostatic force that countered the droplet weight and the drag force exerted by the N_2 gas flow. A constant feedback, based on measurements of the particle position using an imaging camera, adjusted this voltage to maintain the droplet position at a fixed height and at the centre of the intracavity TEM_{00} mode.

Measurements of the ring-down times for both the empty cavity (τ_0) and for the particle levitated at

the centre of the cavity TEM_{00} mode (τ) were recorded during evaporative loss of semi-volatile HT, with typical measurements lasting ~2 hours. The difference in the reciprocals of these ring-down times is proportional to σ_{ext}:

$$\sigma_{ext} = \left(\frac{1}{\tau} - \frac{1}{\tau_0}\right)\frac{L\pi w_0^2}{2c} \qquad (1)$$

In Eqn. (1), L is the cavity length, c is the speed of light, and w_0 is the beam waist of the TEM_{00} Gaussian cavity mode at the location of the trapped particle. Simultaneously, the particle radius was monitored using elastic light scattering. Concurrent with the CRDS measurements, the angular dependence to elastically scattered light intensity for the levitated particle irradiated by a 532-nm laser beam was collected by a high numerical aperture (0.42) objective and imaged using a CMOS camera. These elastic light scattering measurements were recorded over the scattering angular range of ~67.5–112.5°. Particle size was determined from comparisons of these light scattering distributions with Mie theory predictions. In these comparisons, we assumed that $k_{532} = 0$ (with the subscript '532' indicating the optical wavelength in nm) for all droplets presented in this manuscript, while n_{532} was optimized assuming a constant refractive index for the evolving droplet composition using a retrieval approach described in our previous publications.[21] We recognize that these assumptions are contrary to knowledge that nigrosin scatters and absorbs strongly across the visible spectrum. However, we will show in a future publication that these assumptions lead to biases in the retrieved particle radius of only a few nanometres for our weakly light absorbing droplets for which the true n_{532} and k_{532} are expected to reach values up to 1.50 and 0.02, respectively. Moreover, the excellent correspondence between measured and simulated peak positions in extinction cross section demonstrated here and the requirement for small corrections to the retrieved radii of no more than 5.4 nm (see below) further vindicates our particle size analysis approach.

Our approach is currently limited to particles with radii in the range of ~500-1500 nm. The lower size is determined by the Rayleigh limit of charge; when this limit is reached, instantaneous expulsion of mass and charge occurs from the particle to the extent that an isolated droplet is no longer held in the LEQ trap. In principle, this lower size limit can be further reduced by lowering the charge imparted to the initial droplet at the droplet-on-demand dispenser. Although our LEQ can isolate very large (>20 μm radii) particles, the current upper size limit of our CRDS-LEQ approach is a consequence of degraded precision of the recorded ring-down times at larger particle sizes. We hypothesise that the cause is greater amplitude of particle motion within the AC potential of the linear electrodynamic quadrupoles; initial inspection of in-focus images of our droplets suggests that this driven harmonic

motion is larger for particles with radii of ~1500 nm than for those with radii <1000 nm. This greater displacement amplitude from the trap centre moves the particle orthogonally to the axis of the TEM_{00} cavity mode, such that the ring-down time is biased to higher values than those expected for the TEM_{00}-centred particle, creating an exaggerated envelope of ring-down times at larger particle size. In our prior experimental measurements using a Bessel beam optical trap, a smaller envelope of ring-down times was observed at comparable particle radii, suggesting that the Bessel beam optical trap provided tighter droplet confinement in the transverse directions than our current LEQ apparatus. The differences reflect the driven harmonic motion of a particle within the electrodynamic trap, in contrast to passive and stochastic (i.e. Brownian) particle motion within the optical potential of a Bessel laser beam trap. Our initial analysis indicates that in our current LEQ trap, ring-down time measurements of trapped droplets with radii in the range 1000-1500 nm have a standard deviation higher by up to a factor of 2 than our prior measurements with a Bessel beam trap. Further optimisation of our LEQ trap design to improve the stiffness of the trapping potential should remedy this shortcoming of our current apparatus.

Results and Discussion

Figure 2 compares the measured variations in σ_{ext} with particle radius for a droplet composed only of non-absorbing (k = 0 at visible wavelengths) semi-volatile HT, and for two-component droplets composed of mixtures of HT with an absorbing non-volatile dye, nigrosin. At λ = 405 nm, k ~ 0.16 for the nigrosin,[7] and the initial nigrosin mass fractions (w_N) for the binary HT-nigrosin droplets were 0.002 or 0.004. The particle size decreased over time as the semi-volatile HT evaporated, while the concentration of the non-volatile nigrosin increased in the two-component droplets thereby increasing the imaginary refractive index of the droplet at smaller radii. The size-dependent σ_{ext} data reveal broad, oscillatory structure caused by interference of the light rays transmitted through and diffracted around the droplet, with superimposed sharp resonance structures caused by the efficient coupling of the light into resonant modes (referred to as *whispering gallery modes*) of the spherical particle.[22] The remarkable sensitivity of our measurements is evident from the distinguishable impacts of only small increases in the initial chromophore mass concentration corresponding to 0.2 % of the total droplet mass. The whispering gallery modes decrease in amplitude and broaden as the nigrosin concentration increases because of greater absorption losses for these resonant modes (and hence lower quality factor of the resonant mode for the droplet) as k increases.[22] Therefore, the resolved resonance structure in the extinction measurements contains valuable information regarding the absorption efficiency of weakly absorbing aerosol particles and may be compared to optical models to retrieve the complex refractive index.

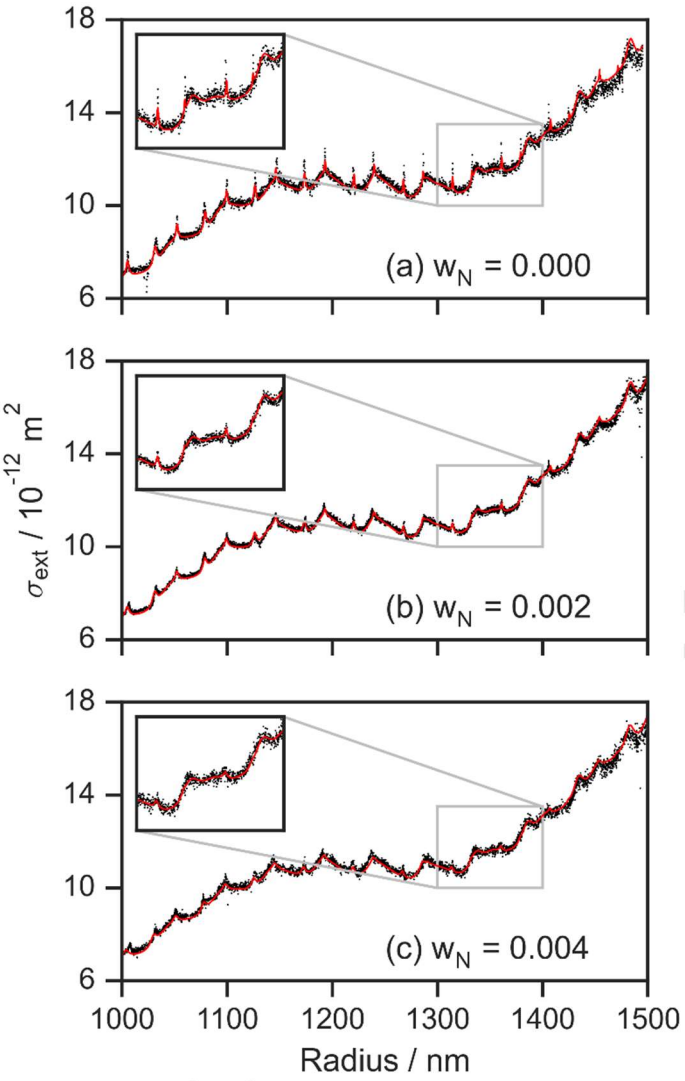

Figure 2. Measured (black points) variation in σ_{ext} with particle radius averaged to a 1 Hz sampling rate for (a) a non-absorbing HT droplet, and for absorbing HT-nigrosin droplets with (b) w_N = 0.002, and (c) w_N = 0.004. The best-fit Mie theory distributions are overlaid (red lines). Insets show expanded regions of the plots to highlight changes in the whispering gallery mode structure with increasing nigrosin absorption.

Previous publications have presented the application of cavity-standing wave Mie theory to retrieve the real refractive index for scattering particles, accounting for the standing wave formed inside a linear optical cavity.[18, 21, 23-25] An envelope in measured σ_{ext} values results from Brownian motion of the particle sampling different phases of this standing wave, with the limits of the envelope corresponding to the particle centred at a node or an antinode. As we will show in a forthcoming publication, the measured σ_{ext} values (recorded at a sampling rate of ~20 Hz) converge to the Mie theory limit for a plane wave when averaged to a sampling rate of 1 Hz, and we exploit this method of data analysis here to improve the accuracy and precision of complex refractive index retrievals. The description of the complex refractive index is optimized by performing a least-squares fit of Mie

theory to the measured 1-Hz cross sections by minimizing the merit function (χ):

$$\chi = \frac{1}{N}\sum_{i=1}^{N}(\sigma_{\mathrm{exp,i}} - \sigma_{\mathrm{Mie,i}})^2 \qquad (2)$$

In Eqn. (2), N is the number of data points, $\sigma_{\mathrm{exp,i}}$ is the measured extinction cross section at a given particle radius, and $\sigma_{\mathrm{Mie,i}}$ is the corresponding calculated Mie theory cross section at the same particle radius. The $\sigma_{\mathrm{exp,i}}$ in this expression is the mean value calculated over a one second interval, and therefore both $\sigma_{\mathrm{exp,i}}$ and the particle radius (which is used in the calculation of $\sigma_{\mathrm{Mie,i}}$) are recorded at a sampling rate of 1 Hz. Our method fits to the magnitudes of the full $\sigma_{\mathrm{exp,i}}$ data set at all particle radii, not just to the positions and widths of the resonant modes, so is not limited by the broadening of these modes with increasing k. Importantly, because the concentrations of HT (volatile) and nigrosin (non-volatile) change with evaporation of the HT component, the refractive indices n and k depend on particle size. The size dependent real refractive index can be described by the empirical expression:

$$n = n_0 + \frac{n_1}{r^3} + \frac{n_2}{r^6} + \cdots + \frac{n_l}{r^{3l}} \qquad (3)$$

In Eqn. (3), r is the droplet radius, n_0 is the real refractive index of the droplet in the limit of infinite size (corresponding here to the n for pure HT), and n_l are coefficients characterizing the size dependence of n for the droplet.[21] For our measurements, only n_1 needs to be varied in this expression to reconcile our Mie theory model calculations with our measured dependence of σ_{exp} on particle size, with all other n_l set to zero. The size dependent imaginary refractive index is defined by:

$$k = \frac{B}{r^3} \qquad (4)$$

In Eqn. (4), B is a constant. This expression has a general form consistent with the mass fraction mixing rule (see Supporting Information). The parameters n_1, B, w_0, and a small multiplicative factor applied to the retrieved particle radius (equivalent to absolute changes in particle radii of less than 5.4 nm) are optimized using a grid search algorithm to minimize the value of χ. Figure 2 compares the best-fit Mie theory distributions to our measurements. Corresponding contour plots for the variation in χ with n_1 and B, for optimized values of w_0 and radius correction factor, are presented in the Supporting Information and demonstrate a single minimum.

For each nigrosin mass fraction (0.000, 0.002, and 0.004), repeat measurements were performed on three separate droplets, with the measured variations in σ_{ext} with particle size provided in the Supporting Information. Figure 3 compares the retrieved size-dependent refractive indices for each droplet studied with predictions from physically based refractive index mixing rule models.

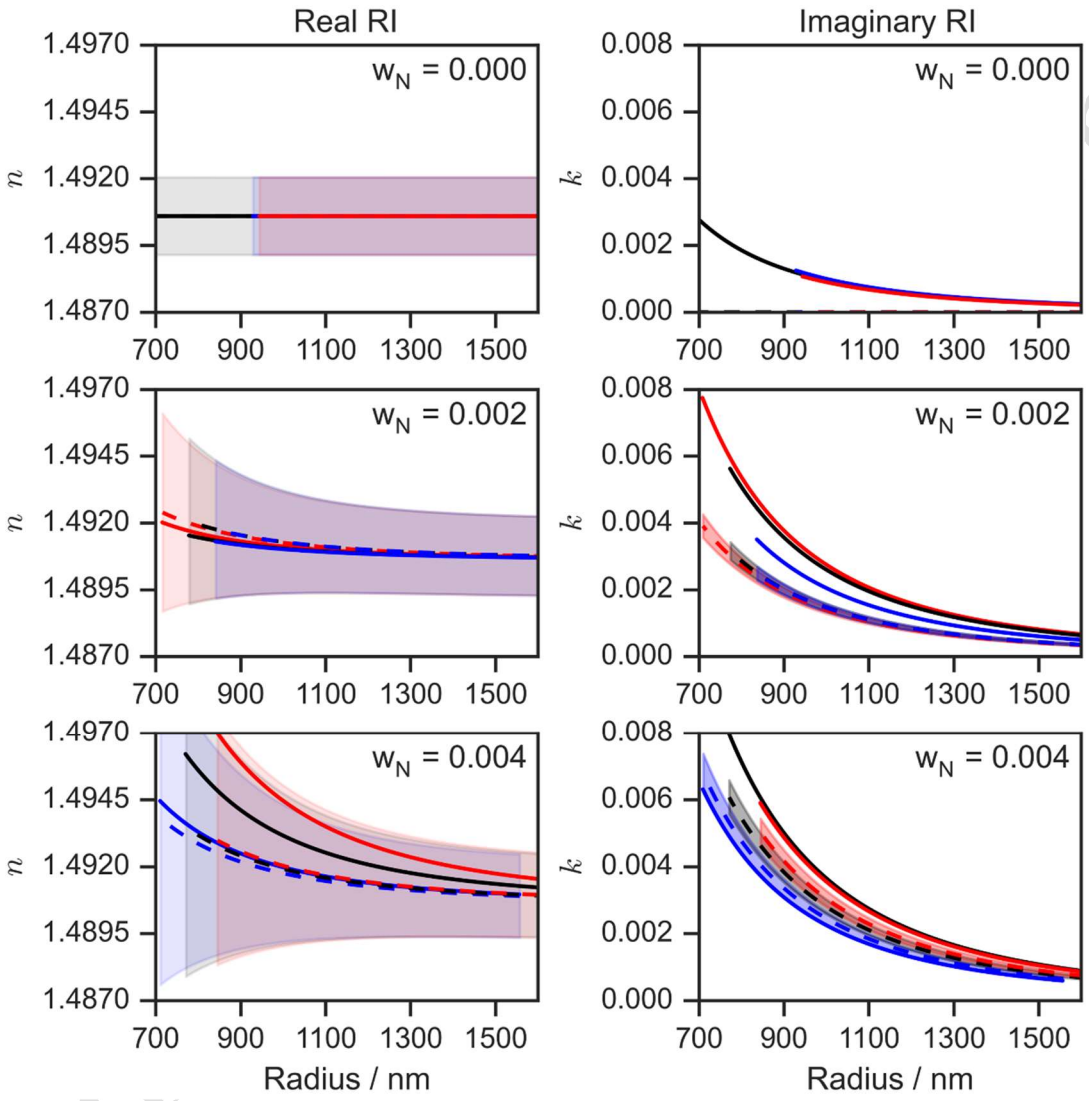

Figure 3. Retrieved (solid lines) and predicted (dashed lines) variation of the *n* and *k* components of the complex refractive indices with particle radius for pure HT droplets (w_N = 0.000; top), and for HT-nigrosin droplets with initial w_N values (corresponding to the solution composition loaded into our droplet dispensers) of 0.002 (middle) and 0.004 (bottom). The shaded envelopes represent the uncertainties in the predicted *n* and *k* values as a function of particle size. The three solid lines of different colours in each panel correspond to the retrieved refractive indices for three separate repeat droplets that were studied for each initial droplet w_N value. Data series extend to different lower values for droplet radii because droplets fell out of the trap stochastically upon evaporation to radii <900 nm.

The mixing rule models used in this work are described in the Supporting Information. The predictions of n and k depend on the initial size of the HT-nigrosin droplets, which could vary from one droplet to the next for sequentially generated droplets. This variability in initial droplet size introduces differences in the size dependent refractive indices, for the predicted as well as the retrieved values. Therefore, Figure 3 shows the size-dependent refractive index predicted for each individual droplet (as indicated by the colour of the data series) using the best estimate of the initial droplet size as determined from angularly resolved elastic light scattering measurements.

The analysis for the pure HT droplets retrieved non-zero B values, corresponding to k values in the range 0.000-0.003 at the largest and smallest particle sizes, respectively. We do not suggest that HT is absorbing from this result. Instead, this non-zero value arises because retrievals of k are sensitive to small errors (of less than 5 nm) in the determined droplet radii that are typical of our experimental approach, causing a small misalignment of the sharp resonance structure in the measured and calculated σ_{ext}. A comprehensive assessment of the impact of particle sizing uncertainties on the fidelity of complex refractive index retrievals is ongoing. This assessment involves the simulation of artificial measurement data sets of ring-down times and particle sizes for evaporating particles of varying absorption strengths (k), with representative measurement uncertainties (including random uncertainties and systematic biases) added to these synthetic data sets prior to the retrieval of n and k using the methods described here. In principle, there is no upper limit to our retrieved k values from measurements of σ_{ext} and particle size. The least squares fit of Mie theory to our σ_{ext} measurements incorporates both the sharper resonance structure and the broader underlying interference structure which becomes progressively damped as k increases. This comprehensive fitting approach is evident from the agreement between the best-fit Mie theory distributions in Figure 2, which match the measurements across the whole extinction cross section range not just at the locations of the resonance peaks. Nonetheless, our approach is limited by the ability to retrieve particle sizes from measured phase functions.

We retrieve n_1 values of less than 10^{-26} m^3 for pure HT droplets, which corresponds to a negligible perturbation of the pure component n for HT by less than ten parts per billion for our droplet sizes. The retrieved k show clear increases as the value of w_N for the initially dispensed solution increases from 0.000 to 0.004 in 0.002 intervals. While the precision of our technique therefore remains high for the complete range of k values studied in this manuscript, the accuracy deteriorates at small k ($w_N \leq 0.002$). This reduction in the accuracy is exaggerated by the $1/r^3$ factor in Eqn. (4), with small changes in B introducing large differences in k at small particle sizes. This effect is particularly significant at smaller w_N because the retrieved B is close to the sensitivity limit. Nevertheless, the

retrieved *n* and *k* show good reproducibility for a given initial HT-nigrosin mass fraction. Differences in these retrievals arise mostly from the variability in the initial size of the particles generated by the droplet dispenser; for a given solution concentration and voltage applied to the droplet-on-demand dispenser, there is a natural variability in the diameter of the ~20 μm sequentially generated droplets of up to a few hundred nanometres. Sources of uncertainty in the mixing rule model predictions are discussed in the Supporting Information.

Conclusions

Here, we have demonstrated that a combination of LEQ trapping and CRDS measurement allows direct, contact free retrievals of both the real and imaginary components of the complex refractive index with high sensitivity for single light absorbing droplets. The outcomes allow predictive mixing rule models to be tested for droplets with constantly evolving compositions. We emphasize the small changes in k of <0.002 resolved in our measurements, with light absorbing aerosols in the atmosphere known to exhibit k values at visible wavelengths of >0.1 for BrC,[26] and up to 0.8 for black carbon.[27] An alternative approach recently developed by Price *et al*. uses a broadband light emitting diode (LED) source to record spectra from a droplet confined in an LEQ.[13] While this method can potentially measure complex refractive indices for aerosol droplets across the bandwidth of the LED, the accuracy and precision of these retrievals is not yet clear for light absorbing droplets with $k > 10^{-3}$. Our method has the advantage of retrieving k values directly by fitting a light scattering model to recorded extinction cross section measurements. It also successfully extracts useful optical information for the sub-micrometre sized particles of most relevance to atmospheric aerosols and can be applied to particles with values of k ($>10^{-4}$) that are most uncertain in climate models. Bluvshtein *et al.* showed that photophoretic spectroscopy could probe single light absorbing particles levitated in an electrodynamic balance to determine k with a sensitivity of $\sim10^{-5}$ for droplets with k in the range $\sim10^{-5}$-10^{-4}.[15] Mie resonance spectroscopy was used to determine the particle size and real component of the refractive index for particles with radii of ~7-13 μm. However, it is not clear that this experimental approach can be extended to particles with radii below 1 μm or to more strongly absorbing particles. Our work demonstrates retrievals of k as high as $\sim10^{-2}$ for particles with radii as small as ~700 nm. Wider advantages of our approach include direct measurement of extinction cross sections that are of relevance to radiative forcing calculations in climate models, both for spherical and non-spherical particles.[14]

Our combination of CRDS and LEQ trapping offers an ideal platform to resolve an array of challenges at the forefront of aerosol science. These challenges include: understanding the impact of mixing state on light absorption, such as the role of coatings on strongly absorbing black carbon particulates;[28, 29]

quantifying the impacts of particle size, viscosity and chemical composition on photoinitiated processes such as photobleaching for which the atmospheric timescales for organic chromophores are not known accurately;[30] and understanding the enhanced reaction rates that are increasingly being reported in aerosols, including for the formation of chromophores relevant to atmospheric BrC aerosols.[31, 32]

Supporting Information

The Supporting Information discusses further the origin of size dependent refractive indices, provides more details of our retrieval algorithm for processing cross section versus particle size data, describes comprehensively the mixing rule models used in this manuscript, our choice of input values to these models, and how uncertainties in the models impact on uncertainties in predicted and retrieved *n* and *k*. In addition, we show plots of the measured variation in σ_{ext} with particle size for each droplet studied with overlaid best-fit Mie theory distributions, and the corresponding contour plots of merit function with variation in n_1 and B for these droplets.

Acknowledgments

Jamie W. Knight and Joanna V. Egan were supported through studentships provided by the EPSRC Centre for Doctoral Training in Aerosol Science (EP/S023593/1). Michael I. Cotterell acknowledges the NERC for the award of an Independent Research Fellowship (NE/S014314/1).

References

1. Feng, Y.; Ramanathan, V.; Kotamarthi, V. R., Brown Carbon: A Significant Atmospheric Absorber of Solar Radiation? *Atmos. Chem. Phys.* **2013,** *13*, 8607-8621.
2. IPCC, Summary for Policymakers. in *Climate Change 2013: The Physical Science Basis. Contribution of Working Group I to the Fifth Assessment Report of the Intergovernmental Panel on Climate Change*, Stocker, T. F.; Qin, D.; Plattner, G.-K.; Tignor, M.; Allen, S. K.; Boschung, J.; Nauels, A.; Xia, Y.; Bex, V.; Midgley, P. M., Eds. Cambridge University Press: Cambridge, United Kingdom and New York, NY, USA, **2013**; pp 1–30.
3. Lin, G.; Penner, J. E.; Flanner, M. G.; Sillman, S.; Xu, L.; Zhou, C., Radiative Forcing of Organic Aerosol in the Atmosphere and on Snow: Effects of SOA and Brown Carbon. *J. Geophys. Res-Atmos.* **2014,** *119*, 7453-7476.
4. Bzdek, B. R.; Reid, J. P.; Cotterell, M. I., Open Questions on the Physical Properties of Aerosols. *Commun. Chem.* **2020,** *3*, 1-4.
5. Lee, J. K.; Banerjee, S.; Nam, H. G.; Zare, R. N., Acceleration of Reaction in Charged Microdroplets. *Q. Rev. Biophys.* **2015,** *48*, 437-444.
6. Yan, X.; Bain, R. M.; Cooks, R. G., Organic Reactions in Microdroplets: Reaction Acceleration Revealed by Mass Spectrometry. *Angew. Chem. Int. Edit.* **2016,** *55*, 12960-12972.
7. Cotterell, M. I.; Szpek, K.; Haywood, J. M.; Langridge, J. M., Sensitivity and Accuracy of Refractive Index Retrievals from Measured Extinction and Absorption Cross Sections for Mobility-Selected Internally Mixed Light Absorbing Aerosols. *Aerosol Sci. Tech.* **2020,** *54*, 1034-1057.

8. Miles, R. E. H.; Rudić, S.; Orr-Ewing, A. J.; Reid, J. P., Sources of Error and Uncertainty in the Use of Cavity Ring Down Spectroscopy to Measure Aerosol Optical Properties. *Aerosol Sci. Tech.* **2011,** *45*, 1360-1375.
9. Zarzana, K. J.; Cappa, C. D.; Tolbert, M. A., Sensitivity of Aerosol Refractive Index Retrievals Using Optical Spectroscopy. *Aerosol Sci. Tech.* **2014,** *48*, 1133-1144.
10. Cremer, J. W.; Thaler, K. M.; Haisch, C.; Signorell, R., Photoacoustics of Single Laser-Trapped Nanodroplets for the Direct Observation of Nanofocusing in Aerosol Photokinetics. *Nat. Commun.* **2016,** *7*, 10941.
11. Diveky, M. E.; Roy, S.; Cremer, J. W.; David, G.; Signorell, R., Assessing Relative Humidity Dependent Photoacoustics to Retrieve Mass Accommodation Coefficients of Single Optically Trapped Aerosol Particles. *Phys. Chem. Chem. Phys.* **2019,** *21*, 4721-4731.
12. Langridge, J. M.; Richardson, M. S.; Lack, D. A.; Brock, C. A.; Murphy, D. M., Limitations of the Photoacoustic Technique for Aerosol Absorption Measurement at High Relative Humidity. *Aerosol Sci. Tech.* **2013,** *47*, 1163-1173.
13. Price, C. L.; Bain, A.; Wallace, B. J.; Preston, T. C.; Davies, J. F., Simultaneous Retrieval of the Size and Refractive Index of Suspended Droplets in a Linear Quadrupole Electrodynamic Balance. *J. Phys. Chem. A.* **2020,** *124*, 1811-1820.
14. Valenzuela, A.; Chu, F.; Haddrell, A. E.; Cotterell, M. I.; Walker, J. S.; Orr-Ewing, A. J.; Reid, J. P., Optical Interrogation of Single Levitated Droplets in a Linear Quadrupole Trap by Cavity Ring-Down Spectroscopy. *J. Phys. Chem. A.* **2021,** *125*, 394-405.
15. Bluvshtein, N.; Krieger, U. K.; Peter, T., Photophoretic Spectroscopy in Atmospheric Chemistry – High-Sensitivity Measurements of Light Absorption by a Single Particle. *Atmos. Meas. Tech.* **2020,** *13*, 3191-3203.
16. Mazurenka, M.; Orr-Ewing, A. J.; Peverall, R.; Ritchie, G. A. D., 4 Cavity Ring-Down and Cavity Enhanced Spectroscopy using Diode Lasers. *Annu. Rep. Prog. Chem., Sect. C: Phys. Chem.* **2005,** *101*, 100-142.
17. Cotterell, M. I.; Willoughby, R. E.; Bzdek, B. R.; Orr-Ewing, A. J.; Reid, J. P., A Complete Parameterisation of the Relative Humidity and Wavelength Dependence of the Refractive Index of Hygroscopic Inorganic Aerosol Particles. *Atmos. Chem. Phys.* **2017,** *17*, 9837-9851.
18. Mason, B. J.; Walker, J. S.; Reid, J. P.; Orr-Ewing, A. J., Deviations from Plane-Wave Mie Scattering and Precise Retrieval of Refractive Index for a Single Spherical Particle in an Optical Cavity. *J. Phys. Chem. A.* **2014,** *118*, 2083-2088.
19. Walker, J. S.; Carruthers, A. E.; Orr-Ewing, A. J.; Reid, J. P., Measurements of Light Extinction by Single Aerosol Particles. *J. Phys. Chem. Lett.* **2013,** *4*, 1748-1752.
20. Gong, Z.; Pan, Y.-L.; Videen, G.; Wang, C., Optical Trapping and Manipulation of Single Particles in Air: Principles, Technical Details, and Applications. *J. Quant. Spectrosc. Radiat. Transf.* **2018,** *214*, 94-119.
21. Cotterell, M. I.; Mason, B. J.; Preston, T. C.; Orr-Ewing, A. J.; Reid, J. P., Optical Extinction Efficiency Measurements on Fine and Accumulation Mode Aerosol using Single Particle Cavity Ring-Down Spectroscopy. *Phys. Chem. Chem. Phys.* **2015,** *17*, 15843-15856.
22. Bohren, C. F.; Huffman, D. R., *Absorption and Scattering of Light by Small Particles*; Wiley-VCH Verlag GmbH: Weinheim, Germany, 1998.
23. Miller, J. L.; Orr-Ewing, A. J., Cavity Ring-Down Spectroscopy Measurement of Single Aerosol Particle Extinction. II. Extinction of Light by an Aerosol Particle in an Optical Cavity Excited by a cw Laser. *J. Chem. Phys.* **2007,** *126*, 174303.
24. Mason, B. J.; Cotterell, M. I.; Preston, T. C.; Orr-Ewing, A. J.; Reid, J. P., Direct Measurements of the Optical Cross Sections and Refractive Indices of Individual Volatile and Hygroscopic Aerosol Particles. *J. Phys. Chem. A.* **2015,** *119*, 5701-5713.
25. Cotterell, M. I.; Preston, T. C.; Orr-Ewing, A. J.; Reid, J. P., Assessing the Accuracy of Complex Refractive Index Retrievals from Single Aerosol Particle Cavity Ring-Down Spectroscopy. *Aerosol Sci. Tech.* **2016,** *50*, 1077-1095.

26. Zarzana, K. J.; De Haan, D. O.; Freedman, M. A.; Hasenkopf, C. A.; Tolbert, M. A., Optical Properties of the Products of α-dicarbonyl and Amine Reactions in Simulated Cloud Droplets. *Environ. Sci. Technol.* **2012,** *46*, 4845-4851.
27. Bond, T. C.; Bergstrom, R. W., Light Absorption by Carbonaceous Particles: An Investigative Review. *Aerosol Sci. Tech.* **2006,** *40*, 27-67.
28. Jacobson, M. Z., Strong Radiative Heating due to the Mixing State of Black Carbon in Atmospheric Aerosols. *Nature* **2001,** *409*, 695-7.
29. Lack, D. A.; Langridge, J. M.; Bahreini, R.; Cappa, C. D.; Middlebrook, A. M.; Schwarz, J. P., Brown Carbon and Internal Mixing in Biomass Burning Particles. *Proc. Natl. Acad. Sci. U. S. A.* **2012,** *109*, 14802-14807.
30. Nissenson, P.; Knox, C. J. H.; Finlayson-Pitts, B. J.; Phillips, L. F.; Dabdub, D., Enhanced Photolysis in Aerosols: Evidence for Important Surface Effects. *Phys. Chem. Chem. Phys.* **2006,** *8*, 4700-4710.
31. Haan, D. O. D.; Corrigan, A. L.; Smith, K. W.; Stroik, D. R.; Turley, J. J.; Lee, F. E.; Tolbert, M. A.; Jimenez, J. L.; Cordova, K. E.; Ferrell, G. R., Secondary Organic Aerosol-Forming Reactions of Glyoxal with Amino Acids. *Environ. Sci. Technol.* **2009,** *43*, 2818-2824.
32. Lee, A. K. Y.; Zhao, R.; Li, R.; Liggio, J.; Li, S.-M.; Abbatt, J. P. D., Formation of Light Absorbing Organo-Nitrogen Species from Evaporation of Droplets Containing Glyoxal and Ammonium Sulfate. *Environ. Sci. Technol.* **2013,** *47*, 12819-12826.

TOC Graphic